Fast approximate 1D modelling and inversion of transient electromagnetic data

Niels B. Christensen*

Department of Geoscience, University of Aarhus, Denmark

ABSTRACT

A novel, fast, and approximate forward modelling routine for time-domain electromagnetic responses is presented. It is based on the separation of the forward problem into a configuration-independent part, mapping conductivity as a function of depth onto apparent conductivity as a function of time, and a configuration-dependent part, i.e., the half-space step response. The response of a layered model is then found as the half-space response for a half-space conductivity equal to the apparent conductivity. The mapping is ten times faster than traditional accurate forward modelling routines, and through stochastic modelling, it is found that the standard deviation of the modelling error is 0.7 %. The forward mapping lends itself to integration in a modern state-of-the-art inversion formulation in exactly the same way as traditionally computed responses, and a field example is included where inversion results using the approximate forward response are compared with those of an accurate forward response for helicopterborne transient electromagnetic data. In addition to being used in its own right in inversion of transient data, the speed and accuracy of the approximate inversion mean that it is well suited for quality control and fast turnaround data delivery of survey results to a client. It can also be used in hybrid inversion formulations by supplying initial iterations and high-quality derivatives in an inversion based on accurate forward modelling.

INTRODUCTION

The transient electromagnetic (TEM) method, particularly airborne TEM, has become one of the most widespread electromagnetic (EM) methods for a wide variety of purposes: mineral prospecting, geotechnical investigations, and hydrogeophysical surveys, to mention the most important areas of application (Fittermann and Stewart 1986; Hoekstra and Blohm 1990; Macnae 1997, 2007; Christensen and Sørensen 1998; Auken *et al.* 2006). Inversion with 1D models, most often with lateral smoothness constraints (Viezzoli *et al.* 2008), is still the most widely used approach to the inversion of TEM data, provided of course that 1D inversion is justified by a moderate lateral rate of change of conductivity. 1D inversion based on accurate forward responses calculated as inverse

Fourier (or Laplace) transforms and Hankel transforms of kernel functions in the frequency (Laplace)/wavenumber domain (Ward and Hohmann 1987) is no longer a heavy computational problem due to the immense increase in cheap computing power. However, Moore's law has also been valid for the increase in the density and overall volume of EM geophysical data. Currently, regional surveys will produce millions, even tens of millions of soundings, and fast inversion based on approximate responses can still be very useful.

In the process of diffusion of transient EM fields into the ground, the diffusion depth and diffusion velocity depend on the subsurface conductivity structure. A number of imaging methods have been suggested, which are based on the variation of the diffusion velocity with conductivity (Nekut 1987; Macnae and Lamontagne 1987; Eaton and Hohmann 1989; Macnae *et al.* 1991). These algorithms find the depth

*E-mail: nbc@geo.au.dk

to an equivalent current filament — an "image" of the source — as a function of time, from which the diffusion velocity and thereby the conductivity can be found. The conductivity is then ascribed to a depth equal to the image depth scaled with an ad hoc factor to produce the best results. In (Macnae and Lamontagne 1987) a number of such images are used instead of just one. Christensen (1995) presented an imaging method based on the all-time apparent conductivity of the step response, a method that was extended to the 2D case in Christensen (1997). The conductivity–depth imaging of Stolz and Macnae (1997) was based on the step response, and the paper by Stolz and Macnae (1998) presented a method for reducing arbitrary waveform TEM data to a step response. Polzer (1985) considered time as a function of the magnetic field and developed a theory for inversion of the arrival time data of a certain amplitude of the magnetic field. Using a linear approximation to the Fréchet kernel, a one-step imaging inverse was developed, where the diffusion depth was scaled according to the arrival time of a reference model, a homogeneous half-space. This scaling of the arrival-time Fréchet kernel is completely equivalent to the one-pass imaging algorithm of Christensen (1995) with scaling according to the all-time apparent conductivity.

The basic principles in 1D approximate inversion have also been extended to approximate 2D and 3D problems. Liu and Asten (1993) presented a fast approximate forward modelling method for 3D thin-sheet models buried in the second layer of a 2-layer earth. Wolfgram, Christensen and Sattel (2003) develop a two-stage approach to approximate 2D inversion of TEM data by combining traditional 1D inversion with an approximate 2D inversion of the 1D conductivity model sections based on an apparent conductivity definition. Their approach was refined by Christensen and Wolfgram (2006) through a formulation of the approximate 2D inversion as a deconvolution, mapping a 1D model section into a 2D model section. Transforming EM fields to magnetic moments, Schaa and Fullagar (2010) have developed a fast approximate 3D inversion scheme capable of including geological constraints.

Some of the fast interpretation algorithms must be characterized as basically data transformations, and many of them involve deconvolution steps. However, deconvolution is an inherently unstable operation, and there is a clear advantage of formulating the approximate inversion problem through an approximate forward mapping (Christensen 2002). In this way, the approximate forward response can be combined with modern inversion schemes and profit from a general and well-understood mathematical formulation.

In this paper, I present a fast and approximate forward modelling routine for time-domain EM responses. The forward mapping is based on a separation of the forward problem into a configuration-independent part, mapping conductivity as a function of depth onto apparent conductivity as a function of time, and a configuration-dependent part, i.e., the half-space step response. The response of a layered model is then found as the half-space response for a half-space conductivity equal to the apparent conductivity. The accuracy is documented through stochastic modelling and analysis of the statistical properties of the modelling error, and the accuracy is compared with that of the more simple approximate mapping of Chistensen (2002) and Christensen, Reid, and Halkjær (2009). Finally, the forward mapping is integrated in an inversion program, and the results of its application on helicopter-borne TEM data acquired with the SkyTEM system from the Broken Hill Managed Aquifer Recharge (BHMAR) project in Australia are compared with inversion with an accurate forward response. Finally, the options of hybrid solutions combining an accurate forward response with approximate derivatives are discussed.

APPROXIMATE FORWARD MODELLING OF TRANSIENT ELECTROMAGNETIC RESPONSES

The new approximate mapping that is the main focus of this paper shares some basic characteristics with the more simple forward modelling routine of Christensen (2002) and Christensen *et al.* (2009). For completeness and due to the simpler approximate mapping playing an important role in the new and more accurate approximate mapping, a short overview of the method is presented in the following.

An approximate forward mapping in time/space domain

A generic and approximate forward modelling for transient step responses was presented by Christensen (2002) and Christensen *et al.* (2009). The entire forward mapping from conductivity as a function of depth $\sigma(z)$ to step response as a function of time $B_L^{step}(t)$ consists of two consecutive steps:

(i) a mapping from conductivity as a function of depth to apparent conductivity as a function of time: $\sigma(z) \to \sigma_a(t)$;

(ii) a substitution of the apparent conductivity $\sigma_a(t)$ into a half-space step response: $B_L^{step}(t) = B_{HSP}^{step}(t, \sigma_a(t))$.

The latter part of the mapping follows from the definition of apparent conductivity as the conductivity of a half-space for which the response will be the same as the layered response at the delay time in question. The first part of the
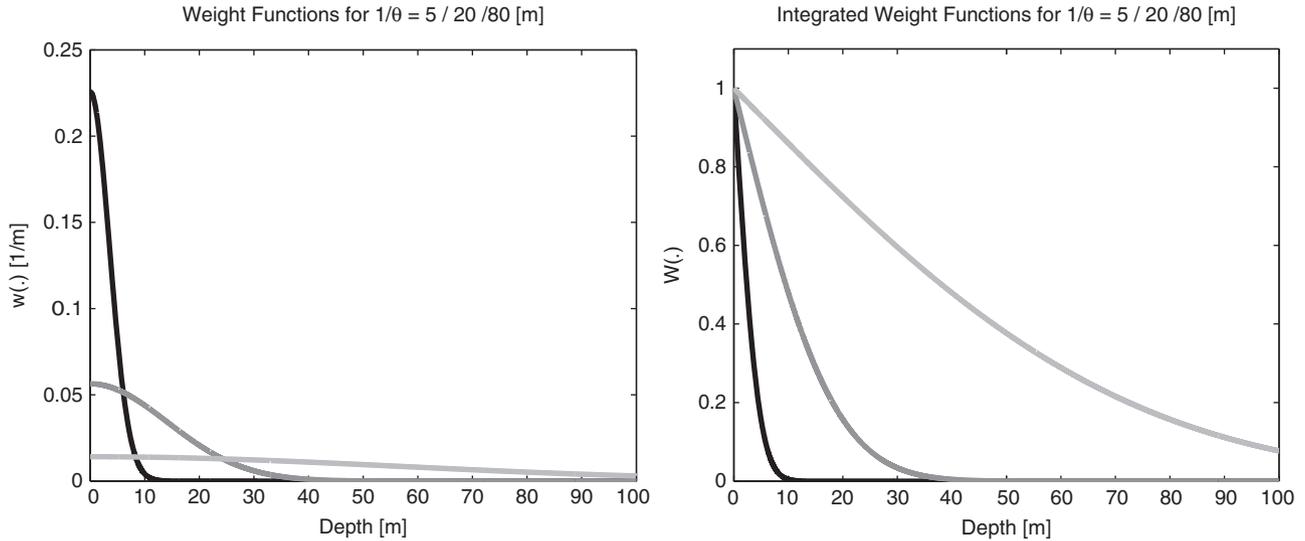
Weight Functions for 1/θ = 5 / 20 /80 [m]

Integrated Weight Functions for 1/θ = 5 / 20 /80 [m]

Figure 1 Plots of the weight function of equation (5) (left) and of the integrated weight function of equation (4) (right) for the three diffusion depths of $1/\theta = 5$ m (black), $1/\theta = 20$ m (dark gray), and $1/\theta = 80$ m (light gray).

mapping, $\sigma(z) \to \sigma_a(t)$, is generic, i.e., it is the same for all transmitter–receiver (Tx–Rx) configurations and all field components, and it is based on an analytic weight function in the time/space domain. In the second mapping, $B_L^{step}(t) = B_{HSP}^{step}(t, \sigma_a(t))$, the half-space step response is specific for the configuration and field component in question. All half-space step responses need only be calculated once at the program start.

This first part of the mapping $\sigma(z) \to \sigma_a(t)$ is given by the integral equation:

$$\sigma_a(t) = \int_0^\infty \sigma(z) w(z, t, \sigma_a(t)) \, dz, \tag{1}$$

where $w(\cdot)$ is a weight function. Notice that $w(\cdot)$ depends on the apparent conductivity. For a layered earth model with N layers having conductivities $\sigma_1, \sigma_2, \ldots, \sigma_N$ and upper layer boundaries $z_1, z_2, \ldots, z_N$; $z_1 = 0$.

$$\sigma_a(t) = \sigma_1 \int_{z_1}^{z_2} w(z, t, \sigma_a(t)) \, dz$$
$$+ \sigma_2 \int_{z_2}^{z_3} w(z, t, \sigma_a(t)) \, dz$$
$$+ \cdots + \sigma_N \int_{z_N}^\infty w(z, t, \sigma_a(t)) \, dz$$
$$= \sigma_1 [1 - W(z_2)] + \sigma_2 [W(z_2) - W(z_3)]$$
$$+ \cdots + \sigma_N [W(z_N)], \tag{2}$$

where $W(z, t, \sigma_a(t))$ is the integrated weight function

$$W(z, t, \sigma) = \int_z^\infty w(z', t, \sigma) \, dz'. \tag{3}$$

The integrated weight function is chosen as

$$W(z, t, \sigma) = \text{erfc}(\theta z), \quad \theta = c\sqrt{\frac{\mu\sigma}{t}}, \tag{4}$$

and the weight function $w(\cdot)$ is consequently given by

$$w(z, t, \sigma) = \frac{2\theta}{\sqrt{\pi}} \exp(-\theta^2 z^2). \tag{5}$$

In Fig. 1, the shapes of w and W are seen as a function of depth for different delay times t.

The weight function defined above has continuous derivatives, an attractive property in numerical manipulations. The parameter c scales the depth extent of the weight function. It is chosen to minimize the difference between the approximate and an accurate forward response of a series of test models, and a value of $c = 1.033$ was found to be the best.

As mentioned above, the (integrated) weight function depends on the apparent conductivity. In this way, the slower diffusion through good conductors and the faster diffusion through poor conductors is properly modelled; the mapping becomes model adaptive. The basic physics of the phenomenon of diffusion of transient fields into the Earth is that the fields diffuse slowly through good conductors and faster through poor conductors. By letting the weight function depend on the apparent conductivity, which is the average conductivity of the part of the subsurface involved in the response,

the modelling mimics the actual physical behaviour of diffusion (Boerner 1990; Christensen 2014).

The price paid for the adaptive property of the modelling, which is absolutely essential for the accuracy, is that the mapping becomes iterative. For any delay time t, the calculations are initialized with some estimate of the apparent conductivity, $\sigma = \sigma_0$, in equation (4), and using equation (2), the apparent conductivity is obtained. The calculations are then repeated by inserting this apparent conductivity into equation (4), and the process is repeated until convergence. Alternatively, observing the scaling properties of $\sigma_a(t)$, i.e., w and W are functions of delay time and half-space conductivity only through the ratio σ/t, it is seen that, although the apparent conductivity calculated after the first step for $\sigma = \sigma_0$: $\sigma_a(t, \sigma_0)$ may not be the apparent conductivity for the delay time t that we eventually wish to obtain, it is the correct apparent conductivity of some delay time, namely, the time t' given by the relation:

$$t'/\sigma_a = t/\sigma_0 \quad \Rightarrow \quad t' = t\frac{\sigma_a}{\sigma_0}. \tag{6}$$

Thus, by shifting the delay times according to (6), no further iterations are needed.

This section has presented an approximate forward mapping procedure for transient methods based on the principles presented in Christensen (2002), however with different and better weight functions. In the following, it is referred to as the simple approximate (SA) mapping. In the next section, an improved approximate modelling algorithm is presented based on the calculation of an apparent conductivity in the wavenumber/space domain in which the above more simple mapping plays the role of initializing the iterative procedure.

An approximate forward mapping in time/wavenumber domain

In this section, an improved version of the approximate forward mapping is presented based on the computation of apparent conductivity in the time/wavenumber domain. The forward mapping follows the same two-step process as outlined earlier, but the mapping from conductivity as a function of depth to apparent conductivity as a function of time, $\sigma(z) \rightarrow \sigma_a(t)$, is different. To avoid the tongue-breaking 'WAvenumber domain approximate' mapping, it will be referred to by the acronym WA. The WA forward response is more accurate than that of the previous approximate mapping and is ~10 times faster than traditional computation methods.

The vertical magnetic field in the frequency domain for a receiver with polar coordinates $(r, -h)$ from a vertical magnetic dipole transmitter at a height H is given as (Ward and Hohmann 1987):

$$H_z(r, z, \omega) = \frac{m}{4\pi} \int_0^\infty [\exp(u_0 h) + \gamma_0 \exp(-u_0 h)]$$
$$\times \exp(-u_0 H) \frac{\lambda^3}{u_0} J_0(\lambda r) \, d\lambda. \tag{7}$$

The first term in the brackets is the primary field, whereas the second term expresses the secondary field. Assuming the quasistatic approximation to be valid ($u_0 = \lambda$), we have:

$$H_z(r, z, \omega) = \frac{m}{4\pi} \int_0^\infty [\exp(2\lambda h) + \gamma_0]$$
$$\times \exp[-\lambda(H + h)] \lambda^2 J_0(\lambda r) \, d\lambda. \tag{8}$$

The kernel function γ_0 (the reflection coefficient) is obtained through recursion from the bottom of the model, the N'th layer, and up:

$$\gamma_n = \exp[-2 \, u_n b_n] \frac{\gamma_{n+1} + \psi_{n+1}}{1 + \gamma_{n+1}\psi_{n+1}}, \quad \gamma_N = 0, \quad b_n = z_n - z_{n-1},$$
$$b_0 = 0$$

$$\psi_{n+1} = \frac{u_n/(i\omega\mu_n) - u_{n+1}/(i\omega\mu_{n+1})}{u_n/(i\omega\mu_n) + u_{n+1}/(i\omega\mu_{n+1})} = \frac{u_n - u_{n+1}}{u_n + u_{n+1}}$$
$$\text{if all } \mu_n = \mu_0 \tag{9}$$

$$u_n = \sqrt{\lambda^2 + i\omega\mu\sigma_n}. \tag{10}$$

Expressing the time-domain field through an inverse Laplace transform with $s = i\omega$ as the Laplace variable, we have for the step response:

$$H_z(r, z, t) = \frac{m}{4\pi} \int_0^\infty \mathcal{L}^{-1}\left\{\frac{1}{s}[\exp(2\lambda h) + \gamma_0]\right\}$$
$$\times \exp[-\lambda(H + h)] \lambda^2 J_0(\lambda r) \, d\lambda. \tag{11}$$

As can be seen from the above equations, to arrive at the transient fields in the time/space domain, we need to perform two consecutive transformations: an inverse Laplace transform to get from Laplace domain to time domain and a Hankel transform to get from wavenumber domain to space domain. The idea behind the WA mapping is to avoid the Hankel transform by calculating the response for only one wavenumber value carefully chosen to maximize the accuracy of the overall computations.

For a homogeneous half-space with conductivity σ, $\gamma_1 = 0$, and γ_0^{HSP} becomes

$$\gamma_0^{HSP} = \psi_1 = \frac{\lambda - u_1}{\lambda + u_1} \Rightarrow 1 + \gamma_0^{HSP} = \frac{2\lambda}{\lambda + \sqrt{\lambda^2 + \mu\sigma s}}$$

$$= \frac{2}{1 + \sqrt{1 + \mu\sigma s/\lambda^2}}. \tag{12}$$

The apparent conductivity in the time/wavenumber domain for a layered model can then be defined as the conductivity for which the time/wavenumber expression for the homogeneous half-space is equal to the one for a layered model, and it is found by equating the right-hand side of equation (11) with the equivalent equation for a homogeneous half-space:

$$\frac{m}{4\pi} \int_0^\infty \mathcal{L}^{-1} \left\{ \frac{1}{s} \left[\exp(2\lambda h) + \gamma_0 \right] \right\}$$
$$\times \exp[-\lambda(H + h)] \, \lambda^2 J_0(\lambda r) \, d\lambda$$

$$= \frac{m}{4\pi} \int_0^\infty \mathcal{L}^{-1} \left\{ \frac{1}{s} \left[\exp(2\lambda h) + \gamma_0^{HSP} \right] \right\}$$
$$\times \exp[-\lambda(H + h)] \, \lambda^2 J_0(\lambda r) \, d\lambda. \tag{13}$$

Removing operators and factors that are identical for the two expressions, we find:

$$\mathcal{L}^{-1} \left\{ \frac{\gamma_0}{s} \right\} = \mathcal{L}^{-1} \left\{ \frac{\gamma_0^{HSP}}{s} \right\} \Rightarrow \mathcal{L}^{-1} \left\{ \frac{1}{s} \left[1 + \gamma_0 \right] \right\}$$

$$= \mathcal{L}^{-1} \left\{ \frac{1}{s} \left[1 + \gamma_0^{HSP} \right] \right\}, \tag{14}$$

where the last derivation is chosen for the sake of numerical convenience.

The inverse Laplace transform of the half-space expression can be found using Equation 29.3.37 of Abramovitz and Stegun (1970):

$$\mathcal{H}_z(u) = \mathcal{L}^{-1} \left\{ \frac{1}{s} \left[1 + \gamma_0^{HSP} \right] \right\}$$

$$= \mathcal{L}^{-1} \left\{ \frac{1}{s} \frac{2}{1 + \sqrt{1 + \mu\sigma s/\lambda^2}} \right\}$$

$$\mathcal{H}_z(u) = (1 + 2u^2) \operatorname{erfc}(u) - \frac{2u}{\sqrt{\pi}} \exp(-u^2),$$

$$u = \lambda d = \lambda \sqrt{t/(\mu\sigma)}. \tag{15}$$

It is seen that γ_0^{HSP} is a function of $(\mu\sigma s/\lambda^2)$ and not of the individual parameters s, σ, and λ, and consequently, the
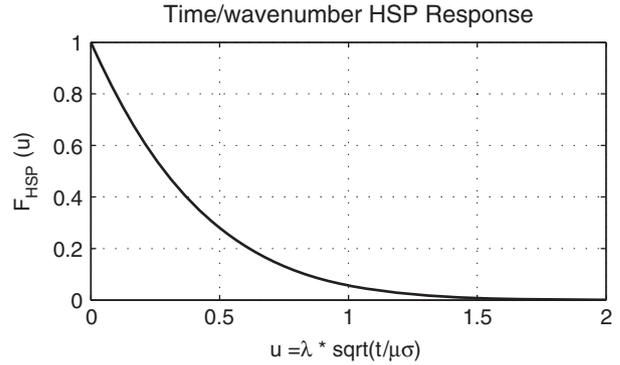

Time/wavenumber HSP Response

Figure 2 Plot of the time/wavenumber domain half-space response.

time-domain expression will be a function of $u = \lambda \cdot d = \lambda \cdot \sqrt{t/(\mu\sigma)}$, where d has the dimension of [m] and is a measure of diffusion distance. A plot of the function $\mathcal{H}_z(u)$ in equation (15) is seen in Fig. 2.

Half-Space responses - with their dependence on geometrical Tx—Rx configuration and field component— can now be calculated by substituting $\mathcal{H}_z(u)$ in the integral in equation (7):

$$H_z(r, z, \omega) = \frac{m}{4\pi} \int_0^\infty \mathcal{H}_z(u) \exp[-\lambda(H + h)] \, \lambda^2 J_0(\lambda r) \, d\lambda$$

$$= \frac{m}{4\pi} \int_0^\infty \left[(1 + 2u^2) \operatorname{erfc}(u) - \frac{2u}{\sqrt{\pi}} \exp(-u^2) \right]$$
$$\times \exp[-\lambda(H + h)] \, \lambda^2 J_0(\lambda r) \, d\lambda. \tag{16}$$

If the transmitter is an extended circular loop with radius a and not a magnetic dipole, we have (Ward and Hohmann 1987):

$$H_z(r, z, t) = \frac{m}{4\pi} \frac{1}{d^3} \int_0^\infty \left[(1 + 2u^2) \operatorname{erfc}(u) - \frac{2u}{\sqrt{\pi}} \exp(-u^2) \right]$$

$$\times \exp\left(-u \frac{H + h}{d} \right) u^2 \left[\frac{J_1\left(u \frac{a}{d} \right)}{\frac{1}{2} u \frac{a}{d}} \right] J_0\left(u \frac{r}{d} \right) du. \tag{17}$$

The approximate modelling procedures presented in the previous section and in here both need the half-space responses for the actual instrument configuration to be calculated at program start and subsequently used for interpolation. The fact that the half-space response is analytically given in the time/wavenumber domain means that the time/space expression can be calculated by performing only one transform, i.e., the Hankel transform from wavenumber to space domain. This transform is performed using the fast Hankel transform

filters by Christensen (1990) and can be calculated to essentially any relevant accuracy for delay times between nanoseconds and hundreds of seconds. This, combined with the fact that the approximate apparent conductivity is accurate for very early and very late times, means that layered responses can be calculated very accurately at practically all times. As mentioned, the half-space responses are calculated only once at the beginning of computations and then stored to serve as lookup tables for subsequent computations.

The above derivations concern the step response. Impulse responses can be found by numerical differentiation in the time/space domain or by differentiating the kernel function $\mathcal{H}_z(u)$ in the time/wavenumber domain with respect to time before the Hankel transformation.

From the above, it is seen that the procedure of finding the apparent conductivity in the time/wavenumber domain for a delay time for any layered model is to recursively compute γ_0 in the Laplace/wavenumber domain, perform an inverse Laplace transform of $[(1 + \gamma_0)/s]$, and then solve to find the conductivity, σ, that will make it identical to the half-space expression. However, the expressions for both the layered model and the homogeneous half-space contain the wavenumber, λ, so there is an apparent conductivity for every wavenumber. Our goal is to find an apparent conductivity in the time/wavenumber domain that is as close an approximation as possible to an accurate apparent conductivity for the step response in the time/space domain, so that the Hankel transform from wavenumber to space domain can be dispensed with. The question is if it is possible to choose a wavenumber so that this goal is achieved. It can be argued that the wavenumber should be the inverse of a typical distance in the space domain, and an obvious choice would then be a wavenumber equal to the inverse of the diffusion distance, i.e., $\lambda_a = 1/d = \sqrt{(\mu\sigma)/t}$. λ_a depends on the ratio between the delay time and the conductivity: t/σ; therefore, it remains to choose a conductivity that is proper for the delay time in question. Again, an obvious choice is the apparent conductivity for that delay time: $\sigma_a(t)$. However, the apparent conductivity is the parameter we wish to find; therefore, the procedure becomes iterative.

To sum up, for every delay time t, the procedure is the following:

(i) Choose an initial apparent conductivity for that delay time, σ_a;
(ii) Choose the wavenumber $\lambda = \lambda_a = 1/\sqrt{t/(\mu\sigma_a)}$;
(iii) For that wavenumber, compute $\mathcal{L}^{-1}\left\{\frac{1}{s}[1 + \gamma_0]\right\}$ for the layered model;

(iv) Solve the equation $\mathcal{L}^{-1}\left\{\frac{1}{s}[1 + \gamma_0]\right\} = \mathcal{H}_z(u)$ to find u;
(v) Find the apparent conductivity so that $\lambda_a\sqrt{t/(\mu\sigma_a)} = u$;
(vi) Repeat steps (1) to (5) until σ_a does not change.

The inverse Laplace transform is obtained using the Gaver–Stehfest algorithm (Knight and Raiche 1982). To reduce the number of iterative steps in the above computation procedure, the initial apparent conductivity must be chosen as close to the final apparent conductivity as possible. This is achieved by using the SA method of calculating the apparent conductivity $\sigma(z) \to \sigma_a(t)$, presented in the previous section. The calculation of the derivatives of the forward response used in an inversion formulation is explained by Christensen *et al.* (2009).

Accuracy of the approximate forward modelling routines

The accuracy of the approximate forward response is determined by the accuracy of the apparent conductivity computation. To verify the approximate modelling approach, 1,000 random 30-layer models with a top layer thickness of 1 m and a depth to the bottom layer of 200 m were created as realizations of a random stochastic process by multiplying the square root of a covariance matrix with a vector of Gaussian-distributed random numbers $\mathbf{r}_\sigma$, with zero mean and unit variance:

$$\log \rho_i = \log <\rho_i^0> + \delta_{\log \rho}\left[\sqrt{\mathbf{C}_m}\,\mathbf{r}_\sigma\right]_i. \tag{18}$$

The covariance matrix of the realizations is based on a broadband covariance function; the same as the one used in the regularization of the inversions in the following sections. Realizations were done in log(resistivity) with a mean of $\log<\rho_0> = \log(50\,\Omega\text{m})$ for all layers and a standard deviation of the perturbation of $\delta_{\log \rho} = 0.6$. The resulting models attain resistivities well below $1\,\Omega\text{m}$ and above $1{,}000\,\Omega\text{m}$. In Figure 3, two sample models are presented, and the responses for an accurate mapping and the SA and WA mappings for the sample models are shown in Fig. 4.

The step responses of the approximate responses were compared with an accurate computation for all 1,000 models using a traditional modelling approach with a Gaver–Stehfest inverse Laplace transform (Knight and Raiche 1982) followed by a Hankel transform (Christensen 1990). In Fig. 5, the standard deviation of the modelling error is shown for the two approximate routines for delay times in the interval from 5 μs to 50 ms. It is seen that the WA mapping performs better than the SA mapping. In Table 1, the statistics of the modelling error averaged over all models and delay times is shown. The standard deviations of the relative error are 1.1% and 0.72%
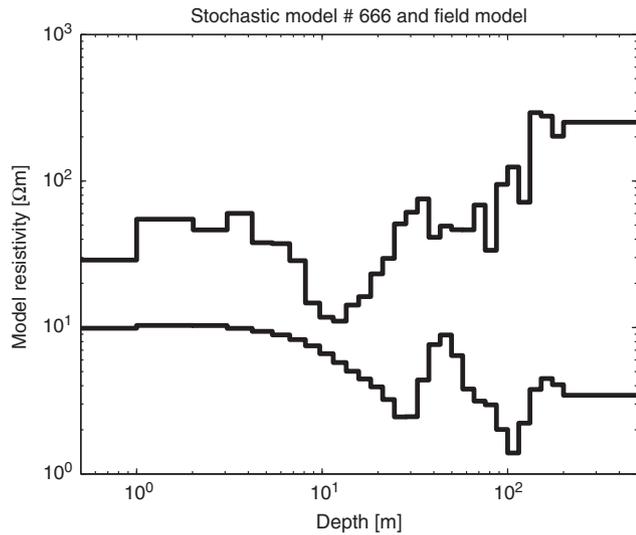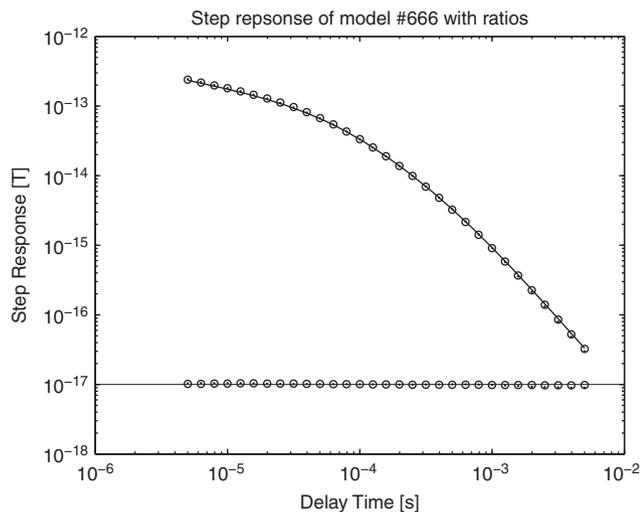
Figure 3 The two sample models: stochastic model #666 (upper curve) and the inversion model from the field example (lower curve) from coordinate E612200, used in the comparison between accurate and approximate responses in Figure 4.

for the SA and the WA mappings, respectively. These standard deviations must be compared with the noise levels of transient data which, in general, are several times higher. The maximum modelling errors are 11% and 5%, for the SA and WA responses, respectively. It is seen that both mappings are well behaved with a mean value of the relative error very close to zero, i.e., they are without bias.

Computation times

The initial calculation of half-space step and impulse responses for 100 different Tx heights at program start takes ~ 0.8 s on one thread of a 2-GHz CPU. Computation times for a 30-layer model for the SA and the WA routines are 0.78 ms and 4.2 ms, respectively. Compared with the computation time of 37.4 ms for the traditional accurate modelling, the approximate mappings offer a speedup of a factor of 48 and 9, respectively. These results are displayed in Table 2, and a further discussion of the computation time issues will follow after the field data inversion example in a following section.

INVERSION FORMULATION

In this section, the use of the approximate forward WA responses in a state-of-the-art inversion formulation is demonstrated. The inversion formulation is exactly the same as the one that would be used with accurate forward responses.

Inversion methodology

There are numerous approaches to the inversion of EM data with a 1D model consisting of horizontal, homogeneous and isotropic layers. The one used with the WA modelling method is a well-established iterative damped least squares approach (Menke 1989). Formally, the model update at the n'th iteration is given by
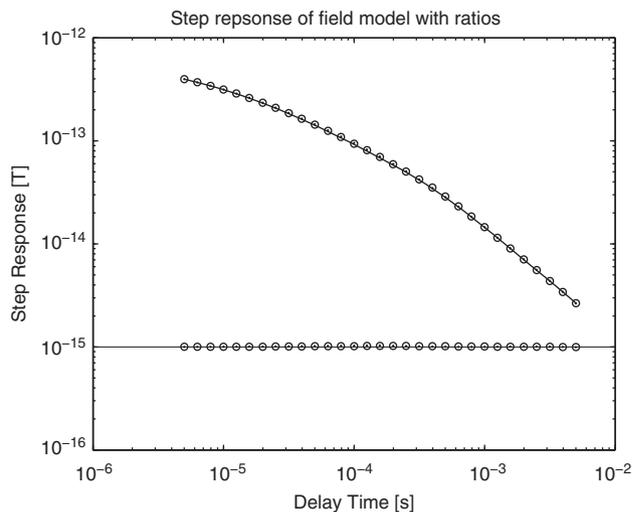

Figure 4 Comparison between the forward step responses of the accurate mapping (full drawn curves), the simple mapping (SA) (dots), and the WA mapping (circles) for stochastic model #666 (left frame), and one of the inversion models of the field example (right frame). In addition to the step responses, the ratios between the SA and the accurate step response (dots) and between the WA response and the accurate step response (circles) multiplied with an appropriate factor are shown in the plots.
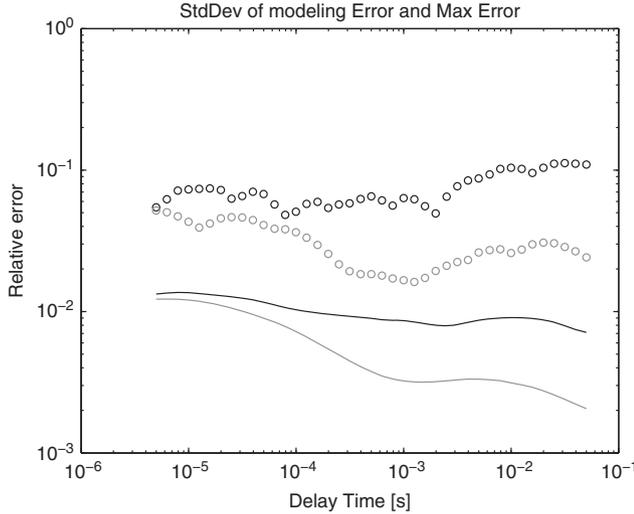
Figure 5 The standard deviations of the forward modelling error of the SA mapping (black) and the WA mapping (gray) as a function of delay time are shown with the full drawn curves. The maximum error for the two mapping are shown as open circles.

Table 1 Statistics of the relative modelling error averaged over all 1,000 models and all 41 delay times. The Table lists the mean, the median, the standard deviation, and the maximum of the absolute value of the relative error for the SA and WA approximate mappings

ERROR STATISTICS	Mean	Median	StdDev	MaxError
SA mapping	−0.00137	−0.00093	0.0106	0.1122
WA mapping	−0.00013	−0.00063	0.0072	0.0519

$$\mathbf{m}_{n+1} = \mathbf{m}_n + \left[\mathbf{G}_n^T \mathbf{C}_{obs}^{-1} \mathbf{G}_n + \frac{1}{\sigma_v^2} \mathbf{C}_m^{-1} \right]^{-1} .$$

$$\left[\mathbf{G}_n^T \mathbf{C}_{obs}^{-1} \left(\mathbf{d}_{obs} - \mathbf{g}\left(\mathbf{m}_n\right) \right) + \mathbf{C}_m^{-1} \left(\mathbf{m}_{prior} - \mathbf{m}_n \right) \right], \qquad (19)$$

where $\mathbf{m}$ is the model vector containing the logarithm of the model parameters, $\mathbf{G}$ is the Jacobian matrix containing the derivatives of the data with respect to the model parameters, T is the matrix transpose, $\mathbf{C}_{obs}$ is the data error covariance matrix, $\mathbf{C}_m$ is a model covariance matrix imposing a vertical smoothness constraint on multi-layer models, $\mathbf{d}_{obs}$ is the field data vector, $\mathbf{g}(\mathbf{m}_n)$ is the nonlinear forward response vector of the n'th model. In this study, as is most often the case, the data noise is assumed uncorrelated, implying that $\mathbf{C}_{obs}$ is a diagonal matrix.

The model parameter uncertainty estimate relies on a linear approximation to the posterior covariance matrix $\mathbf{C}_{est}$ given by

Table 2 Comparison of the computation times for a single forward step responses in the SA and WA approximations and for a traditional accurate code. The table also shows the speedup factors for the approximate responses

COMPUTATION TIMES	Time [ms]	Ratio relative to (3)
(1) SA step response	0.78	48
(2) WA step response	4.2	9
(3) Accurate step response	37.4	1

$$\mathbf{C}_{est} = \left[\mathbf{G}^T \mathbf{C}_{obs}^{-1} \mathbf{G} + \frac{1}{\sigma_v^2} \mathbf{C}_m^{-1} \right]^{-1} , \qquad (20)$$

where $\mathbf{G}$ is based on the model achieved after the last iteration. The analysis is expressed through the standard deviations of the model parameters obtained as the square root of the diagonal elements of $\mathbf{C}_{est}$ (e.g., Inman, Ryu, and Ward 1975).

The model covariance function, $\mathbf{C}_m$, is based on a broadband von Karman covariance function and contains essentially all correlation lengths, and it is used for its superior robustness. For details, see Serban and Jacobsen (2001) and Christensen *et al.* (2009).

AN INVERSION EXAMPLE FROM THE BHMAR DATA SET

I will compare the inversion results of using the WA, the SA, and an accurate forward mapping on data from one line of the helicopterborne transient data from the Broken Hill Managed Aquifer Recharge (BHMAR) project. A total of ∼ 30,000 line km of data were acquired in 2008 with the SkyTEM system (Sørensen and Auken 2004) in a standard duel-moment mode with gate centre times for the low moment between 16 μs and 895 μs and for the high moment between 85 μs and 8.84 ms.

The aim of the BHMAR project was to map fresh and brackish ground water resources in the BHMAR survey area and to point out locations for managed aquifer recharge experiments (Lawrie *et al.* 2012a,b). By implementing managed aquifer recharge, water from annual/biannual large precipitation events would not be lost to evaporation but stored underground for use between the events whereby more water could be left in the Darling–Murray river systems to improve the reliability of domestic and industrial/agricultural water supply and the health of the rivers and the general environment. In addition to the AEM data, the BHMAR project involved borehole induction log data, lithological sampling, hydraulic modelling, assessment of flora and fauna, and an extensive geological interpretation including the effects of neotectonics (Lawrie *et al.* 2012b).
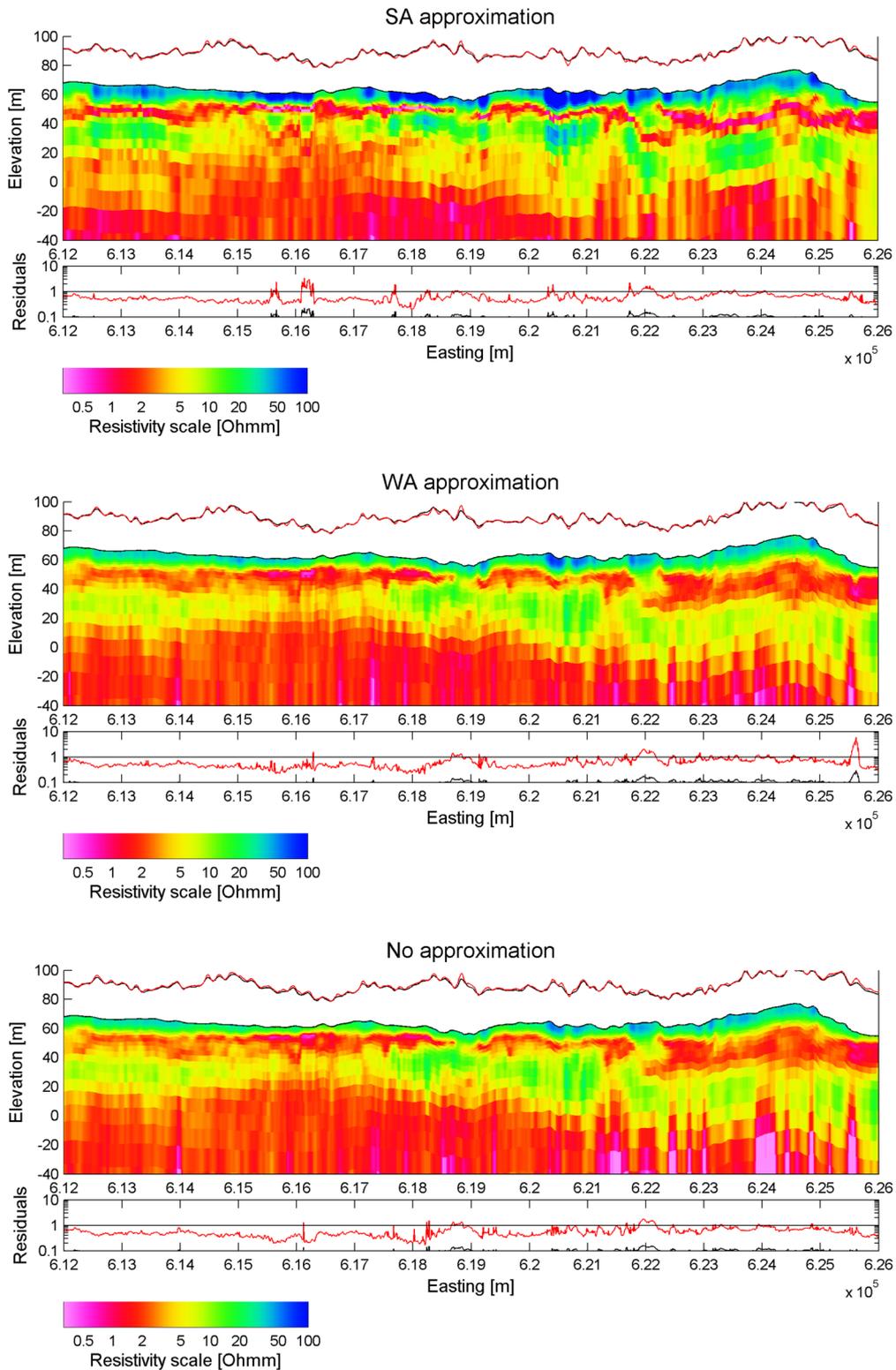
Figure 6 Model sections of a selected interval of a flight line of the BHMAR survey resulting from inversion with the SA approximation (top), the WA approximation (centre), and an accurate inversion scheme (bottom). The top frame of the three subplots is the model section with the measured Tx height in black and the inverted Tx height in red. The total residual (black) and data residual (red) are plotted below the model sections.

Table 3 Comparison of the computation times for the inversion of the 2,125 data sets comprising the model sections displayed in Fig. 6. In addition to the SA, WA, and accurate inversions, the hybrid case of accurate forward responses combined with approximate derivatives is shown. There are 2,125 data sets in each inversion run. Moreover, listed are the speedup factors relative to inversion options (3) and (4)

COMPUTATION TIMES	Time [s]	Ratio relative to (4)	Ratio relative to (3)
(1) SA inversion	444	74	8.6
(2) WA inversion	735	45	5.2
(3) Accurate w/WA derivatives	3,834	8.5	1
(4) Accurate inversion	32,840	1	0.12

The comparison is made using present-day, state-of-the-art, laterally correlated inversion using the Lateral Parameter Correlation (LPC) method (Christensen and Tølbøll 2009; Christensen *et al.*, 2009), i.e., the model sections have been subjected to both vertical and lateral constraints. For all three inversion, the initial model was a half-space with a resistivity of 20 Ωm, a value of $\sigma_v = 4$ (equation (19)) was used for the vertical constraints, and the transmitter height was included as an inversion parameter. In Fig. 6, model sections in a selected interval from the flight line are shown for the SA and WA approximations and for an accurate inversion. Computation times for the laterally uncorrelated inversions for the 2,125 models shown in Fig. 6 are given in Table 2 together with the computation time for a hybrid inversion consisting of an accurate forward response combined with approximate derivatives. All computation times refer to one thread of a 2.5-GHz CPU.

By comparing the three model sections, it is seen that there is hardly any difference between the WA and the accurate inversion; structures and resistivity levels are practically identical. The SA inversion has the same depth to the top of the uppermost good conductor, but the thickness of the top conductor is generally smaller than for the other two inversion schemes. The deeper structures are very similar to the other two. It is also seen that the data residuals of the inversions are much the same in all three cases. The fact that the WA inversion results are almost indistinguishable from those of the accurate inversion makes it a very attractive alternative that can be used not only for an initial overview of the subsurface resistivity distribution but also to deliver the final inversion.

Computation times

Table 3, shows the computation times for the laterally uncorrelated inversions of the 2,125 data sets comprising the model sections of Fig. 6, together with the computation time for a hybrid inversion consisting of an accurate forward response combined with approximate derivatives. All computation times refer to one thread of a 2.5-GHz CPU. In comparison with Table 2, it is obvious that the speedup factors of individual forward responses cannot be maintained when considering inversion. Significant parts of the inversion calculations are used on matrix inversion and the convolutions involved in calculating repetition, low-pass filters of the receiver and the amplifier systems, and integration over the time intervals of the gates.

Table 3 also shows computation times for a hybrid inversion scheme consisting of an accurate forward response combined with approximate derivatives. It is seen that the use of approximate derivatives speeds up the computations with a factor of almost an order of magnitude compared with an all-accurate computation strategy. The models obtained for the two options, indicated as (3) and (4) in Table 3, are in essence identical; therefore, if traditional accurate computations are required for, e.g., contractual reasons, it is a very attractive option to use the approximate derivatives pertaining to the SA and WA approximations. However, a speedup factor of 45 can be obtained with the WA approximation, which also delivers models indistinguishable from the traditional accurate computations.

DISCUSSION AND CONCLUSION

I have presented a fast forward modelling approaches for the calculation of transient electromagnetic (TEM) responses based on a calculation of apparent conductivity in the time/wavenumber domain. The method is about ten times faster than traditional forward responses. Through stochastic modelling, the standard deviations of the relative modelling errors were found to be 0.7%, with mean errors very close to zero, indicating that the error is unbiased. The method was compared with the simpler approximate mapping, which is 50 times faster than that traditional calculations with a modelling error of 1%.

Contemporary airborne TEM systems will often, when used in large surveys, produce millions of data sets, and it

is an appealing option to be able to invert the data using a fast, approximate inversion procedure, particularly one that is as accurate as the one presented in this paper. Data inversion is also one of the best final stages of data quality control, and an option to use a fast, but sufficiently accurate, approximate method makes rapid delivery of survey results to the client feasible within a 24–48 hour time frame.

It is well known that approximate forward responses, when used in an inversion scheme, can produce model artefacts. However, compared with the data error normally attributed to TEM data, the standard deviation of the modelling error is negligible; smaller even than the likely uncertainty on the data error. Moreover, the field example shows that the WA inversion is almost identical to an accurate inversion and that it does not introduce artifacts in the inverted models.

When evaluating and choosing an inversion approach, it is not necessarily an either/or situation between an approximate or an accurate scheme. Although, it is evidently hard to see the difference between the inversion results using an approximate and an accurate forward response, a hybrid scheme can easily be realized in which approximate initial inversions are followed by accurate ones. In this case, only very few computationally more expensive iterations will be needed because of the excellent quality of the approximate inversions. Another hybrid option is to use the approximate derivatives together with an accurate forward modelling routine. It is well documented (Boerner 1990; Farquharson and Oldenburg 1996 1999; Christensen 2014; Christiansen *et al.* 2015) that such hybrid schemes work well, and in this case, the derivatives are quite accurate.

ACKNOWLEDGEMENTS

REFERENCES

Abramowitz M. and Stegun A.S. 1970. *Handbook of Mathematical Functions*. Dover Publications Inc.

Auken E., Pellerin L., Christensen N.B. and Sørensen K. 2006. A survey of current trends in near-surface electrical and electromagnetic methods. *Geophysics* **71**, G249–G260.

Boerner D.E. and Holladay J.S. 1990. Approximate Fréchet derivatives in inductive electromagnetic soundings. *Geophysics* **55**, 1589–1595.

Christensen N.B. 1990. Optimized fast Hankel transform filters. *Geophysical Prospecting* **38**, 545–568.

Christensen N.B. 1995. Imaging of central-loop transient electromagnetic soundings. *Journal of Environmental and Engineering Geophysics* **1**, 53–66.

Christensen N.B. 1997. Electromagnetic subsurface imaging - A case for an adaptive Born approximation. *Surveys in Geophysics* **18**, 477–510.

Christensen N.B. 2002. A generic 1-D imaging method for transient electromagnetic data. *Geophysics* **67**, 438–447.

Christensen N.B. 2014. Sensitivity functions of transient electromagnetic methods. *Geophysics* **79**, E167–E182.

Christensen N.B. and Sørensen K.I. 1998. Surface and borehole electric and electromagnetic methods for hydrogeophysical investigations. *European Journal of Environmental and Engineering Geophysics* **3**, 75–90.

Christensen N.B. and Wolfgram P. 2006. Approximate 2D inversion of airborne TEM data. Australian Earth Science Convention, 2–7 July, Melbourne, Australia.

Christensen N.B. and Tølbøll R.J. 2009. A lateral model parameter correlation procedure for one-dimensional inverse modelling. *Geophysical Prospecting* **57**, 919–929.

Christensen N.B., Reid J.E. and Halkjær M. 2009. Fast, laterally smooth inversion of airborne time-domain electromagnetic data. *Near Surface Geophysics* **7**, 599–612.

Christiansen A.V., Auken E., Kirkegaard C., Schamper C. and Vignoli G. 2015. An efficient hybrid scheme for fast and accurate inversion of airborne transient electromagnetic data. *Exploration Geophysics* **52**.

Eaton P.A. and Hohmann G.W. 1989. A rapid inversion technique for transient electromagnetic soundings. *Physics of the Earth and Planetary Interiors* **53**, 384–404.

Farquharson C.G. and Oldenburg D.W. 1996. Approximate sensitivities for the electromagnetic inverse problem. *Geophysical Journal International* **126**, 235–252.

Farquharson C.G. and Oldenburg D.W. 1999. Approximate sensitivities for multidimensional electromagnetic inversion. In: *Three-Dimensional Electromagnetics*, pp. 256–264. ISBN: 978-1-56080-079-8.

Fittermann D.V. and Stewart M.T. 1986. Transient electromagnetic sounding for groundwater. *Geophysics* **51**, 995–1005.

Hoekstra P. and Blohm M.W. 1990. Case histories of time-domain electromagnetic soundings in environmental geophysics. In: *Geotechnical and Environmental Geophysics*, Vol. 2, Environmental and Groundwater (ed. S.H Ward), pp. 1–16. Society of Exploration Geophysics.

Inman J.R. Jr., Ryu J. and Ward S.H. 1975. Resistivity inversion. *Geophysics* **38**, 1088–1108.

Knight J.H. and Raiche A.P. 1982. Transient electromagnetic calculations using the Gaver-Stehfest inverse Laplace transform method. *Geophysics* **47**, 47–50.

Lawrie K.C., Brodie R.S., Tan K.P., Gibson D., Magee J., Clarke J.D.A. *et al.* 2012a. *BHMAR Project: Data Acquisition, Processing, Analysis and Interpretation Methods. Geoscience Australia Record Geocat 73819*, pp. 520.

Lawrie K.C., Brodie R.S., Dillon P., Tan K.P., Gibson D., Magee J. *et al.* 2012b. *BHMAR Project: Assessment of Conjunctive*

Water Supply Options to Enhance the Drought Security of Broken Hill, Regional Communities and Industries-Summary Report. Geoscience Australia Record 2012/16. pp. 213.

Liu G. and Asten M.W. 1993. Fast approximate solutions of transient EM response to a target buried beneath a conductive overburden. *Geophysics* **58**, 810–817.

Macnae J.C. and Lamontagne Y. 1987. Imaging quasi-layered conductive structures by simple processing of transient electromagnetic data. *Geophysics* **52**, 545–554.

Macnae J.C., Smith R., Polzer B.D, Lamontagne Y. and Klinkert P.S. 1991. Conductivity-depth imaging of airborne electromagnetic step-response data. *Geophysics* **56**, 102–114.

Macnae J. 1997. Developments in broadband airborne electromagnetics in the past decade. In: *Proceedings of Exploration 07 Fifth Decennial International Conference on Mineral Exploration* (ed. B. Milkereit), pp. 387–398.

Macnae J.C. 2007. Developments in broadband airborne electromagnetics in the past decade. In: *Proceedings of Exploration 07. Fifth Decennial International Conference on Mineral Exploration, 9-12 September, Toronto, Canada* (ed. B. Milkereit). pp. 387–398.

Menke W. 1989. *Geophysical Data Analysis: Discrete Inverse Theory*. Academic Press Inc.

Nekut A.G. 1987. Direct inversion of time-domain electromagnetic data. *Geophysics* **52**, 1431–1435.

Polzer B.D. 1985. The interpretation of inductive transient magnetic sounding data. *Research in Applied Geophysics* **36**.

Serban D.Z. and Jacobsen B.H. 2001. The use of broadband prior covariance for inverse palaeoclimate estimation. *Geophysical Journal International* **147**, 29–40.

Schaa R. and Fullagar P.K. 2010. Rapid, approximate 3D inversion of transient electromagnetic (TEM) data. 80th SEG meeting, Denver, USA, Expanded Abstracts, pp. 650–654.

Stolz E. and Macnae J. 1997. Fast approximate inversion of TEM data. *Exploration Geophysics* **28**, 317–322.

Stolz E.M. and Macnae J.C. 1998. Evaluating EM waveforms by singular-value decomposition of exponential basis functions. *Geophysics* **63**, 64–74.

Sørensen K.I. and Auken E. 2004. SkyTEM - A new high-resolution helicopter transient electromagnetic system. *Exploration Geophysics* **35**, 191–199.

Viezzoli A., Christiansen A.V., Auken E. and Sørensen K.I. 2008. Quasi-3D modeling of airborne TEM data by spatially constrained inversion. *Geophysics* **73**, F105–F113.

Ward S.H. and Hohmann G.W. 1987. Electromagnetic theory for geophysical applications. In: *Investigations in Geophysics 3: Electromagnetic Methods in Applied Geophysics* (ed. M.N. Nabighian), pp. 131–311., Society of Exploration Geophysicists.

Wolfgram P., Christensen N.B. and Sattel D. 2003. Approximate 2D inversion of AEM data. In: *16th Geophysical Conference and Exhibition of the Australian Society of Exploration Geophysicists, Adelaidem Australia.*